scientific reports

Check for updates

OPEN

Study of nuclear modification factors of deuteron and anti-deuteron in Pb–Pb collisions at $\sqrt{s_{NN}} = 2.76$ TeV

Feng-Xian Liu[1], Zhi-Lei She[2]✉, Hong-Ge Xu[2], Dai-Mei Zhou[3], Gang Chen[2] & Ben-Hao Sa[4]

The nuclear modification factors (R_{AA}) of d and $\bar{d}$ have been studied using the parton and hadron cascade model plus the dynamically constrained phase space coalescence model in peripheral (40–60%) and central (0–5%) Pb–Pb collisions at $\sqrt{s_{NN}} = 2.76$ TeV with $|y| < 0.5$, $p_T < 20.0$ GeV/c. It is found that the R_{AA} of d, $\bar{d}$ is similar to that of hadrons ($\pi^{\pm}$, p, $\bar{p}$) and the R_{AA} of antiparticles is the same as that of particles. The suppression effect of d is more significant than that of baryons and mesons in the high-p_T region. The suppression of R_{AA} at high-p_T strongly depends on event centrality and mass of the particles, i.e., the central collision is more suppressed than the peripheral collision. Besides, the yield ratios and double ratios for different particle species, and the coalescence parameter B_2 for (d, $\bar{d}$) in pp and Pb–Pb collisions are discussed, respectively. It is observed that the yield ratios and double ratios of d to p and p to π are similar to those of their anti-particles in three different collision systems, suggesting that the suppressions of matter (π^+, p, d) and the corresponding antimatter (π^-, $\bar{p}$, $\bar{d}$) are around the same level.

It is known that quark-gluon plasma(QGP), a new form of nuclear matter characterized by the deconfined state of quarks and gluons, can be produced in heavy-ion collisions at ultra-relativistic energies, such as at the Relativistic Heavy Ion Collider (RHIC) at BNL and Large Hadron Collider (LHC) at CERN. Since a large amount of energy is deposited in the extended QGP matter, it is allowed to create abundant anti-matter ranging from hadrons to light nuclei. Quantitative studies on the production of anti-matter in high energy heavy-ion collisions will shed light on the understanding to the anti-matter to matter asymmetry in our universe. Up to now, numerous experimental results of (anti)hadrons (π^-, $\bar{p}$, $\overline{\Lambda}$, etc.) and (anti)nuclei ($\bar{d}$, ^3He, and $^3_{\overline{\Lambda}}H$, etc.) in pp[1–3] and Pb–Pb[1,2,4–8] collisions at $\sqrt{s_{NN}} = 2.76$ TeV have been reported.

Transverse momentum spectra of various particle species in nucleus–nucleus (A–A) collisions can be applied to study many important properties of the QGP matter. The microscopic process at low-p_T is dominant by the bulk production. In the intermediate p_T region, the baryon-to-meson ratio shows an enhancement[9–11], which is the so called "baryon anomaly" not fully understood so far. For the inclusive particle spectra at high-p_T, transport properties of the QGP matter can be obtained through jet quenching[12–14]. Experimentally, the nuclear modification factor R_{AA} is usually performed to study the jet quenching effect[1,15–19].

The R_{AA}, which compares the p_T distributions of the charged particles in nucleus–nucleus (A–A) collisions to pp collisions, is typically expressed as[2]:

$$R_{AA}(p_T) = \frac{d^2N_{id}^{AA}/d\eta dp_T}{\langle T_{AA}\rangle d^2\sigma_{id}^{pp}/d\eta dp_T}. \quad (1)$$

where N_{id}^{AA} and σ_{id}^{pp} denote the charged particles yield per event in A–A collision and the cross section in pp collision, respectively. The nuclear overlap function T_{AA} is computed based on the Glauber model[20].

The study of the R_{AA} plays an important role in understanding the detailed mechanism by which hard partons lose energy traversing the medium[21]. Recent experimental data of R_{AA} in Pb–Pb collision from ALICE[1,2,17,18,22] and CMS[19] experiments have been published for a range of charged hadrons. Compared with R_{AA} of hadrons

[1]School of Mathematics and Physics, Hubei Polytechnic University, Huangshi 435003, China. [2]School of Mathematics and Physics, China University of Geosciences, Wuhan 430074, China. [3]Institute of Particle Physics, Central China Normal University, Wuhan 430079, China. [4]China Institute of Atomic Energy, P.O. Box 275(10), Beijing 102413, China. ✉email: shezhilei@cug.edu.cn

(charged particles, π, k, p, etc.), R_{AA} of light (anti)nuclei is not well explained in high energy A–A collision experiments. Therefore we think the properties of R_{AA} of (anti)hadrons and (anti)nuclei in Pb–Pb collisions deserve to be further using theoretical models.

Presently, there are many successful phenomenological models widely used to describe the production of hadrons and light nuclei in relativistic heavy-ion collisions[23,24], such as the Ultra-relativistic Quantum Molecular Dynamics (UrQMD) approach[25], a Multiphase Transport (AMPT) model[26], and the Simulating Many Accelerated Strongly interacting Hadrons (SMASH) approach[27]. For the light (anti)nuclei production in terms of their yields, yield ratios, p_T-spectra, flow, etc., either the coalescence models[28–35] or the statistical thermal approaches[36–39] are usually employed. The lightest nuclear cluster, i.e., deuterons, has been especially studied to shed light on the nuclei formation process. For example, Ref.[31] shows the spectra and elliptic flow of deuterons by the IEBE-VISHNU hybrid model with AMPT initial conditions + coalescence model at RHIC and LHC energies. In Ref.[38] a hydrodynamics + hadronic transport approach is adopted to explore the microscopic evolution process of deuteron production via the $\pi d \leftrightarrow \pi pn$ reaction in Pb–Pb collisions at LHC energy.

In this paper, the production and transverse momentum (p_T) of final state (anti)hadrons ($\pi^+, \pi^-, p, \bar{p}$) are simulated by PACIAE model[40] in pp and Pb–Pb collisions at $\sqrt{s_{\rm NN}} = 2.76$ TeV. And then the dynamically constrained phase-space coalescence (DCPC) model[41] is applied to deal with the production and properties of light (anti)nuclei ($d, \bar{d}$). Previous results of light (anti)nuclei production for both pp[41,42] and A–A[43–49] collisions in relativistic energy region, including spectra, energy dependence, scaling property, centrality dependence have been obtained using this framework. In the rest of this paper, we will investigate the properties of nuclear modification factors (R_{AA}) of (anti)hadrons and (anti)deuteron in Pb–Pb collisions at $\sqrt{s_{\rm NN}} = 2.76$ TeV with the same approach.

The paper is organized as follows: In "Models" section, we concisely introduce the PACIAE and DCPC model. In "Results and discussions" section, our numerical calculation results of the R_{AA} for (anti)hadrons and (anti) deuteron are presented and compared with the available experimental data at LHC. In "Conclusions" section, a brief summary is provided.

Models

The PACIAE model[40,50,51] based on PYTHIA 6.4[52], is designed and expanded to be feasible for lepton-nucleus and nuclear-nucleus (p–p, p–A and A–A) collisions. Compared with PYTHIA , the partonic rescattering process is introduced after the creation of parton initial conditions, while the hadronic rescattering may happen after the hadronization of QCD matter in PACIAE model. In this model, the entire collision process contains four evolution stages as follows:

Firstly, the partonic initial states are created by simplifying nucleus–nucleus collision into numerous nucleon-nucleon (NN) collisions according to the collision geometry, Glauber model and NN total cross section. Each NN collision is described by the PYTHIA model generating quarks and gluons for further evolution. A partonic initial state, also considered as quark-gluon matter (QGM), is reached when all NN collisions are exhausted. Secondly, the parton rescattering proceeds via the $2 \rightarrow 2$ parton-parton scattering described by the lowest-leading-order perturbative QCD (Lo-pQCD) cross sections[53]. Thirdly, the hadronization process is treated through the Lund string fragmentation approach[52]. Finally, the hadron rescattering is carried out till the exhaustion of hadron-hadron collision pairs or the hadronic freeze-out. One can see[40] for the detail.

Unlike previous works within PACIAE2.0[40], here we choose the upgraded version PACIAE2.2[54] to calculate the nuclear modification factors (R_{AA}). In this version, several new physics features such as the final-state transverse momentum anisotropy, a new effective string tension mechanism etc., have been included. Also, an additional chiral magnetic effect(CME) initial charge separation mechanism[55,56] is introduced. Recently, this approach also has be employed to calculate the "correspondence principle" of R_{AA} between of hadrons and its component quarks in A–A collisions[57].

PACIAE does not assume equilibrium, such as the other transport (cascade) models UrQMD[25] and/or AMPT[26]. It just simulates dynamically the whole relativistic heavy-ion collision process from the initial partonic stage to the hadronic final state via the parton evolution, hadronization, and hadron evolution according to copious dynamical ingredients assumptions introduced reasonably. Therefore it is parallel to the experimental nucleus–nucleus collision. These dynamics correctly describe the particle, energy, and entropy developments, etc., while the intensive thermodynamical quantities are not defined in this non-equilibrium regime.

In the theoretical papers, the yield of nuclei usually is calculated in two steps: First, the nucleons are calculated by the transport model. Then, the nuclei are calculated by the phase-space coalescence model based on the Wigner function[58] or by the statistical model[59]. We proposed a dynamically constrained phase-space coalescence (DCPC) model[41] to calculate the yield of (anti-)nuclei after the transport model simulations.

From quantum statistical mechanics[60], one can not precisely define both position $\vec{q} \equiv (x, y, z)$ and momentum $\vec{p} \equiv (p_x, p_y, p_z)$ of a particle in six-dimensional phase space because of the uncertainty principle, $\Delta\vec{q}\Delta\vec{p} \sim h^3$. One can only say this particle lies somewhere within a six-dimensional quantum box or state of volume of $\Delta\vec{q}\Delta\vec{p}$ volume element in the six-dimensional phase space corresponds to a state of the particle. Therefore, one can estimate the yield of a single particle[60] by

$$Y_1 = \int_{E_a \le H \le E_b} \frac{d\vec{q}d\vec{p}}{h^3}, \tag{2}$$

where H denotes the Hamiltonian of energy function and E_a, E_b are the lower and upper energy threshold, respectively. Analogously, one can compute the yield of the light (anti)nuclei containing N particles with the following integral:

$$Y_N = \int \cdots \int_{E_a \le H \le E_b} \frac{d\vec{q}_1 d\vec{p}_1 ... d\vec{q}_N d\vec{p}_N}{h^{3N}}. \tag{3}$$

Such as, the yield of a *p*-*n* cluster or deuteron in the DCPC model can be calculated by

$$Y_d = \int \cdots \int \delta_{12} \frac{d\vec{q}_1 d\vec{p}_1 d\vec{q}_2 d\vec{p}_2}{h^6}, \tag{4}$$

$$\delta_{12} = \begin{cases} 1 & \text{if} \quad 1 \equiv p, 2 \equiv n; \\ & m_d - \Delta m \le m_{inv} \le m_d + \Delta m, \\ & q_{12} \le D_0; \\ 0 & \text{otherwise.} \end{cases} \tag{5}$$

where

$$m_{inv} = \sqrt{(E_1 + E_2)^2 - (\vec{p}_1 + \vec{p}_2)^2}. \tag{6}$$

Here, the variables $\vec{q}$ and $\vec{p}$ are the coordinates and momentum of the particle in the center-of-mass frame system at the moment after hadronic completion. m_d denotes the mass of deuteron, and Δm refers to its mass uncertainty; E_1, E_2 and $\vec{p}_1, \vec{p}_2$ denote the energies and momenta of the two particles (p and n); the $q_{12} = |\vec{q}_1 - \vec{q}_2|$ is the distance between the two particles. The deuteron is produced by the combination of proton and neutron after the final hadrons have been produced using the PACIAE model.

In Eq. (2), the energy function H satisfies $H^2 = (\vec{p}_1 + \vec{p}_2)^2 + m_{inv}^2$ and the energy threshold satisfies $E_{a,b}^2 = (\vec{p}_1 + \vec{p}_2)^2 + (m \mp \Delta m)^2$. Thus, the dynamic constraint condition $m - \Delta m \le m_{inv} \le m + \Delta m$ in Eq. (5) is equivalent to $E_a \le H \le E_b$[61]. Hence we may use the constraint condition $m - \Delta m \le m_{inv} \le m + \Delta m$, instead of $E_a \le H \le E_b$, to estimate the yield of particle clusters by the phase-space integral.

Results and discussions

At first, we can obtain the final-state particles in *pp* and Pb–Pb collisions using the PACIAE model[40]. In this simulation, the hadrons are created on the assumption that hyperons heavier than Λ are already decayed, and most of model parameters are fixed on the default values given in PYTHIA6.4[52]. We determine the *K* factor, parj(1,2,3) for primary hadrons in PACIAE model by fitting to the ALICE pions and protons transverse momentum spectra data[2]. Here, the *K* factor is introduced to include the higher order and the nonperturbative corrections, parj(1) is the suppression of diquark-antidiquark pair production compared with the quark-antiquark pair production, parj(2) is the suppression of strange quark pair production compared with $u(d)$ quark pair production, and parj(3) is the extra suppression of strange diquark production compared with the normal suppression of a strange quark. The fitted values of $K = 2$ (default value is 1 or 1.5), parj(1) = 0.15 (0.1), parj(2) = 0.50 (0.3), and parj(3) = 0.60 (0.4) for *pp* collisions as well as $K = 2$, parj(1) = 0.15, parj(2) = 0.38, and parj(3) = 0.65 for Pb–Pb collisions are used in later calculations. Then we generate charged pions and (anti)protons transverse momentum spectra by PACIAE model with $|y| < 0.5$ and $0 < p_T < 20$ GeV/c at $\sqrt{s_{\rm NN}} = 2.76$ TeV, in *pp* collisions as shown in Fig. 1 and Pb–Pb collisions for centrality bin of 0–5% and 40–60% as shown in Fig. 2, respectively.

Then the yields and transverse momentum spectra of (anti)deuteron were calculated by the dynamically constrained phase-space coalescence model (DCPC) in *pp* and Pb–Pb collisions at $\sqrt{s_{\rm NN}} = 2.76$ TeV according to the final hadronic states from the PACIAE model. Here, we choose the model parameter $D_0 = 3$ fm and $\Delta m = 0.42$ MeV/c in *pp* and Pb–Pb collisions[46]. In the end, we can compare the model calculations of the nuclear modification factors for (anti)hadrons and light (anti)nuclei in Pb–Pb collisions at $\sqrt{s_{\rm NN}} = 2.76$ TeV to experimental data and study the quenching effect in relativistic heavy-ion collisions.

In Fig. 1, the transverse momentum spectra of charged pions, and (anti)protons computed by PACIAE model (the open symbols) in *pp* collisions at $\sqrt{s} = 2.76$ TeV within rapidity $|y| < 0.5$ were used to fit model parameters with ALICE results[2] (the solid symbols). In addition, the transverse momentum spectra of (anti)deuteron calculated by the PACIAE + DCPC model simulation (the open symbols) in *pp* collisions at $\sqrt{s} = 2.76$ TeV within rapidity $|y| < 0.5$ are also shown in the Fig. 1, which is in agreement with the known ALICE results[3]. The experimental data can be reproduced well at $p_T > 4$ GeV/c, while a certain discrepancy exists between experimental data and model results at $p_T < 4$ GeV/c, especially for low p_T pions and intermediate p_T protons due to overestimate or underestimate of their spectrum. Therefore, the present model is required for further improvement to a better description of transverse momentum spectra of the final-state hadrons.

Similarly, Fig. 2 shows the transverse momentum spectra of charged pions, and (anti)protons calculated by PACIAE + DCPC model (open symbols) in Pb–Pb collisions at $\sqrt{s_{\rm NN}} = 2.76$ TeV for different centrality bins of 0–5% and 40–60% within rapidity $|y| < 0.5$ confronted with ALICE results[2] (the solid symbols). One can see from Fig. 2 that for $p_T < 3.0$ GeV/c, the spectra in central collisions becomes harder and there is a mass dependent effect. Both protons and pions transverse momentum spectra are well described by our model in different centrality bins. Then the transverse momentum spectra of deuteron computed by the PACIAE + DCPC model simulation (the open symbols) in Pb–Pb collisions at $\sqrt{s_{\rm NN}} = 2.76$ TeV in both central and peripheral collisions are in agreement with the ALICE data[6,7], but a large discrepancy of deuterons compared to pions and protons as shown in the lower panel of Fig. 2. This phenomenon can be explained that, according to the deuteron production mechanism, deuteron can be formed by coalescence of $(p + n)$. Hence the mass ordering as well as the superposition of the difference of data-to-model ratios for proton and neutron, can lead to the discrepancy of Data/Model ratios for deuterons more larger than that for pions and protons.

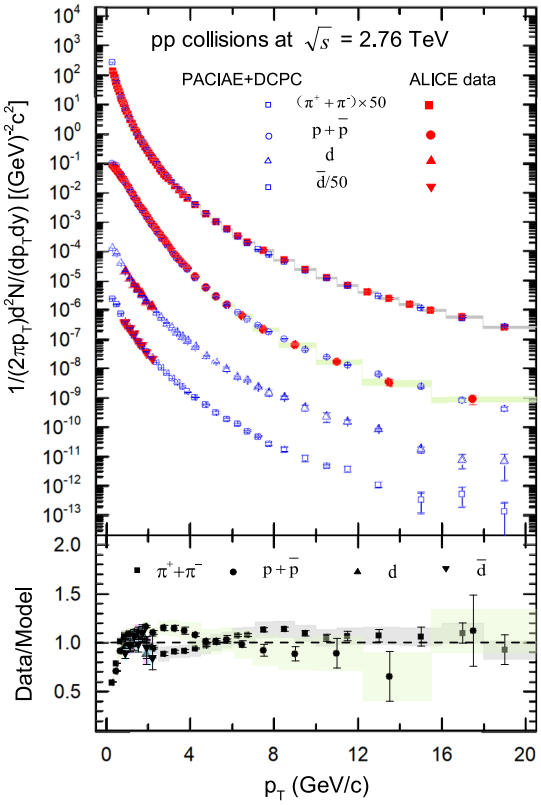

Figure 1. The transverse momentum spectra of charged pions, (anti)protons, and (anti)deuteron computed by PACIAE + DCPC model (the open symbols) in pp collisions at $\sqrt{s} = 2.76$ TeV, compared with ALICE results[2,3] (the solid symbols). The vertical lines (error bars) show the statistical uncertainty and the shaded areas represent the systematic uncertainty of the ALICE results. The spectra have been scaled by the factors listed in the legend for clarity. The lower panels show the deviations of the spectra predicted by our model to ALICE data.

The nuclear modification factor R_{AA} for pion, proton and deuteron is shown in Fig. 3 (the open symbols). Figure 3a–c show the distribution of the nuclear modification factor R_{AA} for the π^+, p, and d compared to their antiparticles π^-, $\bar{p}$, and $\bar{d}$, in two different centrality bins. Figure 3d–f show the distribution of R_{AA} versus p_T for combined $\pi^+ + \pi^-$, $p + \bar{p}$, and $d + \bar{d}$.

From Fig. 3, one can see that the distribution of the nuclear modification factor R_{AA} for different particle species and different centrality increases with p_T value, reaches a peak, and then decreases with transverse momentum p_T, indicating a unified energy loss mechanism is acting on all the different particle species including nuclei at high transverse momentum. And the depression effect of central collision event are more significant than that of peripheral collision, due to a stronger medium modification effect in central collisions.

We notice that the R_{AA} factors of different particles exhibit a maximum for the intermediate p_T range, $2.0 < p_T < 4.0$ GeV/c, a feature generically called the "Cronin effect" (growth of high-transverse momentum cross sections with nuclear size)[62]. For the shapes of the R_{AA}, it may be explained that at high-p_T the R_{AA} is suppressed owing to the strong partonic energy loss effect. While at low and intermediate p_T region, it can be understood by radial boosts and/or the Cronin Effect[63]. For the low-p_T region, radial boosts may push particles to higher p_T region, leading to a smaller R_{AA}. For the enhancement at intermediate p_T, the Cronin effect due to the multiple nucleon-nucleon scattering effect[64] tends to transform the longitudinal momentum into the transverse momentum, and finally results in a pronounced peak at the intermediate p_T region.

Next, we can see from Fig. 3a–c that the R_{AA} distribution of antihadrons and antinuclei are the same with that of corresponding hadrons and nuclei, showing that the R_{AA} suppression or quenching effect on matter and antimatter is the same in high energy Pb–Pb collisions. It is worth noting, as shown in Fig. 3c,f, that the suppression or quenching effect in the high transverse momentum region is more significant for nuclei than in meson and baryons, this may be interpreted as the nuclei spectra are changed more dramatic due that the so-called "pion wind effect" (protons rescatter with pions gaining higher transverse momentum) induced by hadron rescattering process and baryons-antibaryons $B\bar{B} \rightarrow$ mesons annihilation reactions[38] influence the transverse momentum spectra of component nucleons for nuclei at high-p_T region.

The solid markers in Fig. 3c–e represent the experimental data[2,3,6] compared with our simulation results. It is observed that the R_{AA} results of the $\pi^+ + \pi^-$, $p + \bar{p}$ and d from our simulation are comparable to those of the ALICE data at $p_T < 10.0$ GeV/c within the current errors in Fig. 3c–e; while as $p_T > 10.0$ GeV/c, our simulation is off the data by a small factor due to the particles spectra are slight underestimated at this region. It should

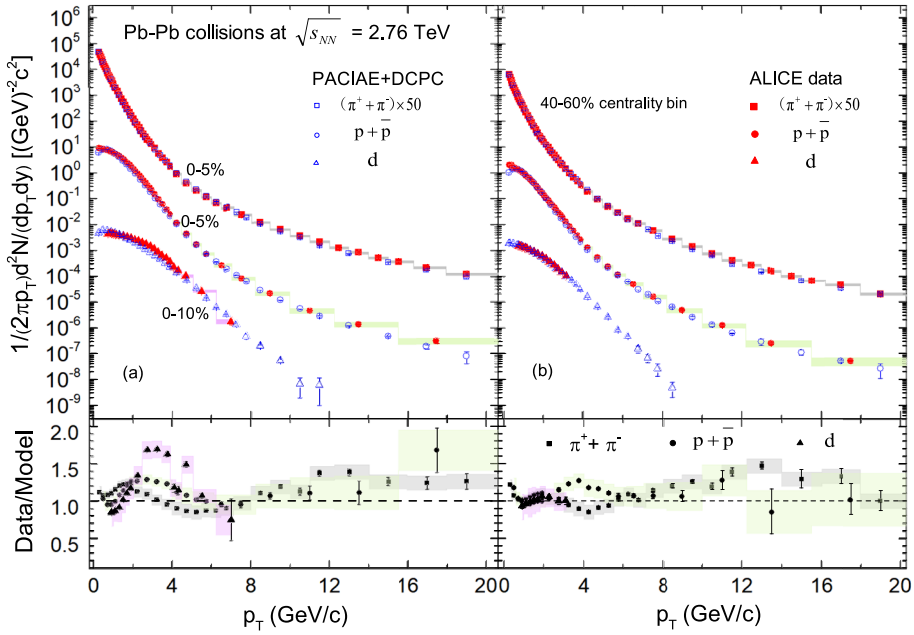

Figure 2. The transverse momentum spectra of charged pions, (anti)protons, and deuteron are presented by PACIAE + DCPC model (the open symbols) in Pb–Pb collisions at $\sqrt{s_{NN}} = 2.76$ TeV, compared with ALICE results[2,6,7] (the solid symbols), (**a**) in centrality bin of 0–5% for $\pi^+ + \pi^-$, $p + \bar{p}$ and 0–10% for d, (**b**) in centrality bin of 40–60%, respectively. The vertical lines (error bars) show the statistical uncertainty and the shaded areas represent the systematic uncertainty of the experimental results. The spectra of charged pions have been scaled by the factors 50 for clarity. The lower panels show the deviations of the spectra predicted by our model to ALICE data.

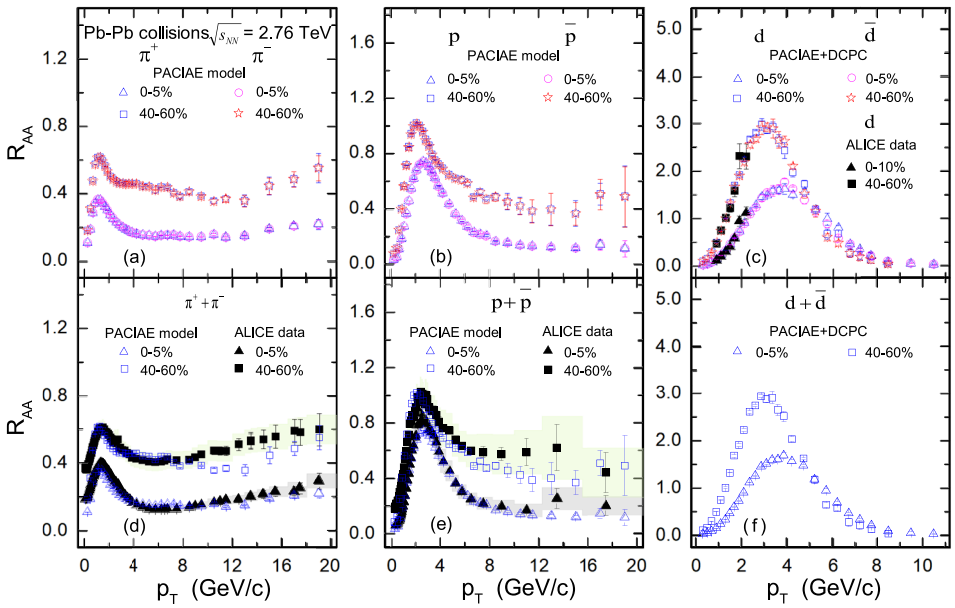

Figure 3. The nuclear modification factor R_{AA} are calculated by PACIAE + DCPC model (the open symbols) for different particle species in 0–5% most central and 40–60% peripheral Pb–Pb collision events at $\sqrt{s_{NN}} = 2.76$ TeV, as a function of p_T. The ALICE results (the solid markers) for comparison were taken from Ref.[2] for panel (**d**) and (**e**), and were computed using the data from Ref.[3,6] for panel (**c**). The vertical lines (error bars) show the statistical uncertainty and the shaded areas represent the systematic uncertainty of the experimental results.

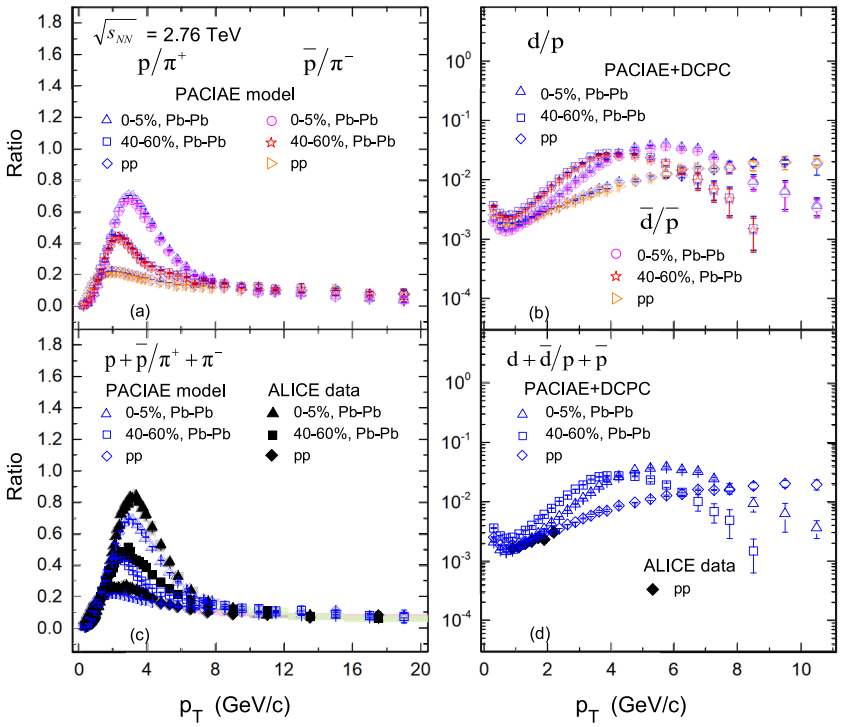

Figure 4. The ratios of (anti)proton to charged-pion and (anti)deuteron to (anti)proton computed by PACIAE + DCPC model (the open symbols) as a function of p_T in pp collisions, as well as the most central (0–5%) and peripheral (40–60%) Pb–Pb collisions at $\sqrt{s_{NN}} = 2.76$ TeV, respectively. Here, ALICE results (the solid markers) for comparison were take from Ref.[2] in panel (**c**), and were computed with the data from Ref.[2,3] in panel (**d**). The vertical lines (error bars) show the statistical uncertainty and the shaded areas represent the systematic uncertainty of the experimental results.

be mentioned that the ALICE data R_{AA} of d used for comparison in Fig. 3c were calculated according to Eq. (1) based on the experimental data taken from Ref.[3] for pp collisions and Ref.[6] for Pb–Pb collisions.

We also perform a particle ratio study versus p_T for (anti)proton to charged pion and (anti)deuteron to (anti) proton in this model. Figure 4a,b, display the ratio distributions of p/π^+, $\bar{p}/\pi^-$, d/p, and $\bar{d}/\bar{p}$, respectively. It's easy to see that the distributions of the ratio for $p/\pi^+, d/p$ are similar to $\bar{p}/\pi^-, \bar{d}/\bar{p}$ in pp collisions, central and peripheral Pb–Pb collisions, suggesting a common suppression behavior for the matter and antimatter.

We note that a minimum value of ratios at $p_T = 0.7$ GeV/c in Fig. 4b, indicating that deuterons are difficult to produce by protons and neutrons at this region. For the decrease trend below $p_T = 0.7$ GeV/c, it may be caused by the emitting source volume increases and density of corresponding components decreases[47]. When $p_T > 0.7$ GeV/c, the ratios increases with p_T value, reaches a peak, and then decreases at higher-p_T, which may be a joint result of the dynamics constraints (nuclei with large momentum hard to form) and density of component nucleons ($p-n$ correlation hard to occur if density is small).

The ratio distributions of $(p+\bar{p})/(\pi^+ + \pi^-)$ and $(d+\bar{d})/(p+\bar{p})$ are shown in Fig. 4c,d. It can be seen that for the central and peripheral Pb–Pb collisions, the ratio grows to a maximum value at $p_T \sim 3.0$ GeV/c for $(p+\bar{p})/(\pi^+ + \pi^-)$ and $p_T \sim 5.0$ GeV/c for $(d+\bar{d})/(p+\bar{p})$, then decreases as p_T increases. In Fig. 4c,d, the solid markers show the ALICE results[2] for comparison. Obviously, the $(p+\bar{p})/(\pi^+ + \pi^-)$ ratio in our simulation shows a similar structure to that in data. The ALICE data $(d+\bar{d})/(p+\bar{p})$ used for comparison in Fig. 4d were computed using data $(p+\bar{p})$ taken from Ref.[2] and data $(d+\bar{d})$ from Ref.[3].

To quantify the similarity of the suppression, the double R_{AA}^D ratio were defined, such as the double ratio R_{AA}^D of protons to pions is defined as follows[1]:

$$R_{AA}^D(p_T) = \frac{R_{AA}^{(p+\bar{p})}(p_T)}{R_{AA}^{(\pi^+ + \pi^-)}(p_T)}, \tag{7}$$

where $R_{AA}^{(\pi^+ + \pi^-)}$ and $R_{AA}^{(p+\bar{p})}$ denote the R_{AA} for the charged pion and proton, respectively. This double ratios constructed using the particle ratios may be properly handled that the dominant correlated systematic uncertainties are between particle species and not between different collision systems.

Figure 5 shows the double R_{AA}^D ratios of protons $(p, \bar{p}, p+\bar{p})$ to pions $(\pi^+, \pi^-, \pi^+ + \pi^-)$ and deuterons $(d, \bar{d}, d+\bar{d})$ to protons $(p, \bar{p}, p+\bar{p})$, as a function of p_T, calculated by PACIAE + DCPC in the most central (0–5%) and peripheral (40–60%) Pb–Pb collisions at $\sqrt{s_{NN}} = 2.76$ TeV, respectively. We can see from Fig. 5, that the R_{AA}^D for all particle combinations are generally increasing at low-p_T and decreasing at high-p_T. And

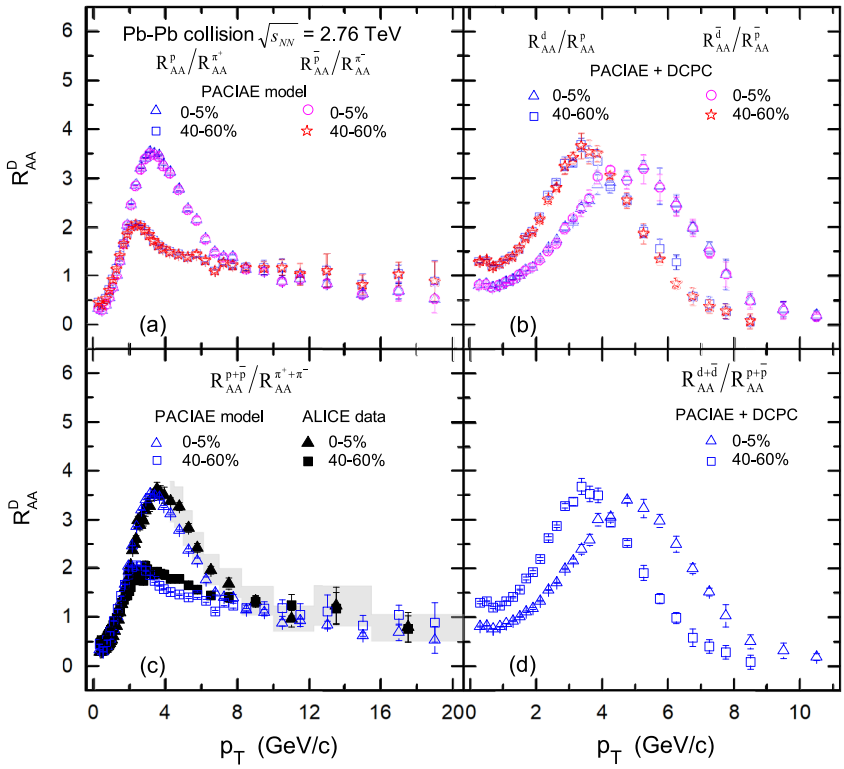

Figure 5. The double ratios R_{AA}^{D} of (anti)proton to charged-pion and (anti)deuteron to (anti)proton computed by PACIAE + DCPC model (the open symbols) as a function of p_T in pp collisions, as well as in Pb–Pb collisions of the centrality bins of 0–5% and 40–60% at $\sqrt{s_{NN}} = 2.76$ TeV, respectively. Here, ALICE data (the solid markers) for comparison in panel (**c**), at $p_T > 4.0$ GeV/c, were taken directly from Ref.[1]; at $p_T < 4.0$ GeV/c, were calculated using the data from Ref[2]. The vertical lines (error bars) show the statistical uncertainty and the shaded areas represent the systematic uncertainty of the experimental results.

comparing Fig. 5a,c with Fig. 5b,d, we can also conclude that the suppression effect of the double R_{AA}^{D} ratio of deuteron to proton is more significant than that of proton to pion, as $p_T > 8$ GeV/c. For $p_T < 8$ GeV/c the double ratios $R_{AA}^{(p+\bar{p})}/R_{AA}^{(\pi^++\pi^-)}$ in 40–60% peripheral centrality are much lower than that of 0–5% centrality bin. This may reflect a different centrality dependence in magnitude for the two particle species, i.e., for the pions, the suppression becomes more pronounced in the more central collision bins, as expected from the increasingly dense final-state system and longer average path-lengths traversed by hard-scattered partons before fragmenting into final hadrons[19]. However, protons appear to be similar suppressed from peripheral to central events at this p_T region.

Besides, it is clear that, as shown in Fig. 5a,b, the distribution of the double R_{AA}^{D} ratios for p to π^+ and d to p are the same as that of corresponding antimatter $\bar{p}$ to π^- and $\bar{d}$ to $\bar{p}$, which indicates that matter and corresponding antimatter have the same suppression characteristics. Meanwhile, from Fig. 5c it can be seen that the distribution of the results R_{AA}^{D} from computed by model simulation are consistent with the ALICE data[1,2]. It should be noted that the experimental values of double ratios $R_{AA}^{(p+\bar{p})}/R_{AA}^{(\pi^++\pi^-)}$ used for comparison in Fig. 5c, when $p_T < 4.0$ GeV/c, were calculated using data $R_{AA}^{(\pi^++\pi^-)}$ and $R_{AA}^{(p+\bar{p})}$ taken from Ref.[2], and when $p_T > 4.0$ GeV/c, were taken directly from Ref.[1].

To gain more insight into deuteron production above, we also investigate the coalescence parameter B_2 variation based on deuteron and proton data. The coalescence parameter B_2 plays an important role in depicting the difficulty of (anti-)deuteron production in high energy collisions. And we can obtain the coalescence parameter $B_2\,(p_T)$ for pp and Pb–Pb collisions, from the transverse momentum spectra shown in Figs. 1 and 2, which is inspected as follows[38]:

$$B_2(p_T) = \frac{\frac{1}{2\pi}\frac{d^3N_d}{p_T dp_T dy}\big|_{p_T^d = 2p_T^p}}{\left(\frac{1}{2\pi}\frac{d^3N_p}{p_T dp_T dy}\right)^2}. \tag{8}$$

In the Fig. 6, one can see that the distribution of coalescence parameter B_2 exhibits an increasing trend with the increase of transverse momentum per nucleon (p_T/A). This increase may be qualitatively explained by position-momentum correlations caused by a radially expanding source[6,7,65].

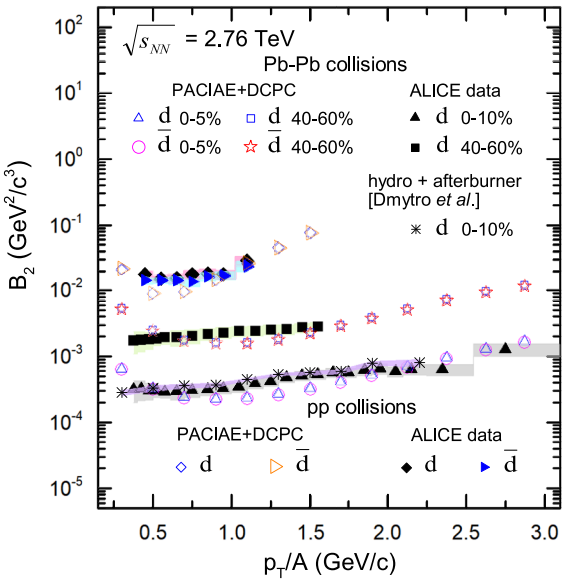

Figure 6. The coalescence parameter B_2 of (anti-)deuteron, extracted from PACIAE + DCPC model simulation, is compared to ALICE data in pp[3] and Pb–Pb[6,7] collisions of the most central and peripheral centrality at $\sqrt{s_{\rm NN}} = 2.76$ TeV, respectively. The vertical lines (error bars) show the statistical uncertainty and the shaded areas represent the systematic uncertainty of the experimental results.

To understand this increase better we analyse the coalescence mechanism on deuterons by proton and neutron pairs in our DCPC model, the invariant mass m_{inv} of deuterons can be calculated by Eq. (6) to be $m_{inv} = \sqrt{(E_1 + E_2)^2 - p_T^2 - p_z^2}$, if we assume that the energy of nucleon E_1, E_2, and longitudinal momentum p_z remain constant, a lower value for m_{inv} will be obtained at the higher-p_T, leading to the dynamic constraint condition Δm in Eq. (3) is much easier to be satisfied. Hence the relative number density probability of p–n pairs enhances at high-p_T, which ultimately results in the increase of coalescence parameter B_2 with p_T/A.

Furthermore, deuteron coalescence parameter B_2 extracted from the PACIAE + DCPC calculation is quite consistent with the ALICE data[3,6,7] and the hydrodynamics + hadronic afterburner approach results[38]. One can also see from Fig. 2 that the transverse momentum spectra of proton and deuteron are slightly underestimated, especially for the deuteron in 0–10% Pb–Pb collisions. Hence aiming to get a good B_2 coalescence parameter, an improved result for the (anti-)proton and (anti-)deuteron spectra should be supplied.

Incidentally, to better understand the nuclear modification factors (R_{AA}), especially for the origin of the enhancements at intermediate p_T region, we have tested the influence of the effects (such as transverse momentum anisotropy, chiral magnetic effect etc.) and the physics input model parameters (including K Factor, parj(1,2,3)) introduced in the PACIAE model, it turns out that these considerations are not enough to explain the origin of the enhancement.

Conclusions

In the paper, we have studied the transverse momentum spectra of deuteron ($d, \bar{d}$), as well as hadrons ($\pi^+ + \pi^-$ and $p + \bar{p}$) at scaled midrapidity $|y| < 0.5$ in pp collisions, most central (0–5%) and peripheral (40–60%) Pb–Pb collisions by PACIAE + DCPC model. The key model parameters are determined by fitting pion and proton transverse momentum spectra data. Then, the nuclear modification factors (R_{AA}) of charged pions, (anti)protons, and (anti)deuteron, as well as, their yield ratios, double R^D_{AA} ratios and the coalescence parameter B_2 with $|y| < 0.5$ in peripheral (40–60%) and central (0–5%) Pb–Pb collisions at $\sqrt{s_{NN}} = 2.76$ TeV have been studied using the PACIAE + DCPC model. It is found that the R_{AA} distribution of light (anti)nuclei ($d, \bar{d}$) is similar to that of hadrons ($\pi^{\pm}, p, \bar{p}$), but is more significant for nuclei than meson and baryons at high-p_T region, and the R_{AA} of anti-particles is the same as that of particles. The suppression of R_{AA} at high-p_T strongly depends on event centrality and mass of the particles. Besides, the coalescence parameter B_2 with transverse momentum per nucleon (p_T/A) calculated by PACIAE + DCPC model exhibits an increasing trend.

Most of the results predicted by our theoretical model are consistent with existing experimental results, while others are somewhat different, such as the R_{AA} distribution of charged pions at the high-p_T. Therefore, the present model is required for further improvement to a better description of transverse momentum spectra of the final-state hadrons and light nuclei. An upcoming meaningful improvement that the production of light nuclei and hypernuclei will be directly implanted into the hadronization stage, can be better employed to study the nuclear modification factors (R_{AA}) of nuclei in nuclear collisions.

Received: 3 July 2021; Accepted: 10 January 2022
Published online: 02 February 2022

References

1. Abelev, B. *et al.* Production of charged pions, kaons and protons at large transverse momenta in *pp* and Pb–Pb collisions at $\sqrt{s_{NN}} = 2.76$ TeV. *Phys. Lett. B* **736**, 196 (2014).
2. Adam, J. *et al.* Centrality dependence of the nuclear modification factor of charged pions, kaons, and protons in Pb–Pb collisions at $\sqrt{s_{NN}} = 2.76$ TeV. *Phys. Rev. C* **93**, 034913 (2016).
3. Acharya, S. *et al.* Production of deuterons, tritons, ^{3}He nuclei, and their antinuclei in *pp* collisions at $\sqrt{s} = 0.9$, 2.76, and 7 TeV. *Phys. Rev. C* **97**, 024615 (2018).
4. Abelev, B. *et al.* Centrality dependence of π, K, and p production in Pb–Pb collisions at $\sqrt{s_{NN}} = 2.76$ TeV. *Phys. Rev. C* **88**, 044910 (2013).
5. Abelev, B. *et al.*K^0_S and Λ production in Pb–Pb collisions at $\sqrt{s_{NN}} = 2.76$ TeV. *Phys. Rev. Lett.* **111**, 222301 (2013).
6. Adam, J. *et al.* Production of light nuclei and anti-nuclei in *pp* and Pb–Pb collisions at energies available at the CERN Large Hadron Collider. *Phys. Rev. C* **93**, 024917 (2016).
7. Acharya, S. *et al.* Measurement of deuteron spectra and elliptic flow in Pb–Pb collisions at $\sqrt{s_{NN}} = 2.76$ TeV at the LHC. *Eur. Phys. J. C* **77**(10), 658 (2017).
8. Adam, J. *et al.*$^3_\Lambda$H and $^{\overline{3}}_{\overline{\Lambda}}\overline{\mathrm{H}}$ production in Pb–Pb collisions at $\sqrt{s_{NN}} = 2.76$ TeV. *Phys. Lett. B* **754**, 360 (2016).
9. Adcox, K. *et al.* Suppression of hadrons with large transverse momentum in central Au+Au collisions at $\sqrt{s_{NN}} = 130$ GeV. *Phys. Rev. Lett.* **88**, 022301 (2001).
10. Adler, C. *et al.* Centrality dependence of high-p_T hadron suppression in Au+Au collisions at $\sqrt{s_{NN}} = 130$ GeV. *Phys. Rev. Lett.* **89**, 202301 (2002).
11. Adams, J. *et al.* Transverse-momentum and collision-energy dependence of high-p_T hadron suppression in Au+Au collisions at ultrarelativistic energies. *Phys. Rev. Lett.* **91**, 172302 (2003).
12. Gyulassy, M. & Plümer, M. Jet quenching in dense matter. *Phys. Lett. B* **243**(4), 432 (1990).
13. Gyulassy, M. & Wang, X. N. Multiple collisions and induced gluon bremsstrahlung in QCD. *Nucl. Phys. B* **420**, 583 (1994).
14. Wang, E. K. & Wang, X. N. Jet tomography of hot and cold nuclear matter. *Phys. Rev. Lett.* **89**, 162301 (2002).
15. Adcox, K. *et al.* Formation of dense partonic matter in relativistic nucleus–nucleus collisions at RHIC: Experimental evaluation by the PHENIX Collaboration. *Nucl. Phys. A* **757**(1), 184 (2005).
16. Adams, J. *et al.* Experimental and theoretical challenges in the search for the quark-gluon plasma: The STAR Collaboration's critical assessment of the evidence from RHIC collisions. *Nucl. Phys. A* **757**(1), 102 (2005).
17. Aamodt, K. *et al.* Suppression of charged particle production at large transverse momentum in central Pb–Pb collisions at $\sqrt{s_{NN}} = 2.76$ TeV. *Phys. Lett. B* **696**(1), 30 (2011).
18. Abelev, B. *et al.* Centrality dependence of charged particle production at large transverse momentum in Pb–Pb collisions at $\sqrt{s_{NN}} = 2.76$ TeV. *Phys. Lett. B* **720**(1), 52 (2013).
19. Chatrchyan, S. *et al.* Study of high-p_T charged particle suppression in Pb–Pb compared to pp collisions at $\sqrt{s_{NN}} = 2.76$ TeV. *Eur. Phys. J. C* **72**(3), 1945 (2012).
20. Alver, B. *et al.* Importance of correlations and fluctuations on the initial source eccentricity in high-energy nucleus–nucleus collisions. *Phys. Rev. C* **77**, 014906 (2008).
21. Casalderrey-Solana, J. & Salgado, C. A. Introductory lectures on jet quenching in heavy ion collisions. *Acta Phys. Pol. B* **38**(12), 3731 (2007).
22. Acharya, S. *et al.* Transverse momentum spectra and nuclear modification factors of charged particles in *pp*, p-Pb and Pb–Pb collisions at the LHC. *J. High Energy Phys.* **2018**(11), 13 (2018).
23. Chen, J. H. *et al.* Antinuclei in heavy-ion collisions. *Phys. Rep.* **760**, 1 (2018).
24. Braun-Munzinger, P. & Dönigus, B. Loosely-bound objects produced in nuclear collisions at the LHC. *Nucl. Phys. A* **987**, 144 (2019).
25. Bass, S. *et al.* Microscopic models for ultrarelativistic heavy ion collisions. *Prog. Part. Nucl. Phys.* **41**, 255 (1998).
26. Lin, Z. W. *et al.* A multi-phase transport model for relativistic heavy ion collisions. *Phys. Rev. C* **72**, 064901 (2005).
27. Weil, J. *et al.* Particle production and equilibrium properties within a new hadron transport approach for heavy-ion collisions. *Phys. Rev. C* **94**, 054905 (2016).
28. Shah, N. *et al.* Production of multistrange hadrons, light nuclei and hypertriton in central Au + Au collisions at $\sqrt{s_{NN}} = 11.5$ and 200 GeV. *Phys. Lett. B* **754**, 6 (2016).
29. Liu, P. *et al.* Production of light nuclei and hypernuclei at high intensity accelerator facility energy region. *Nucl. Sci. Technol.* **28**, 55 (2017).
30. Zhu, L. L., Ko, C. M. & Yin, X. J. Light (anti-)nuclei production and flow in relativistic heavy-ion collisions. *Phys. Rev. C* **92**, 064911 (2015).
31. Zhao, W. B. *et al.* Spectra and flow of light nuclei in relativistic heavy ion collisions at energies available at the BNL relativistic heavy ion collider and at the CERN large hadron collider. *Phys. Rev. C* **98**, 054905 (2018).
32. Sombun, S. *et al.* Deuteron production from phase-space coalescence in the UrQMD approach. *Phys. Rev. C* **99**, 014901 (2019).
33. Sun, K. J., Ko, C. M. & Dönigus, B. Suppression of light nuclei production in collisions of small systems at the Large Hadron Collider. *Phys. Lett. B* **792**, 132 (2019).
34. Wang, R. Q. *et al.* Different production sources of light nuclei in ultra-relativistic heavy-ion collisions. *Chin. Phys. C* **43**, 024101 (2019).
35. Liu, H. *et al.* Light nuclei production in Au + Au collisions at $\sqrt{s_{NN}} = 5 - -200$ GeV from JAM model. *Phys. Lett. B* **805**, 135452 (2020).
36. Vovchenko, V., Dönigus, B. & Stöecker, H. Multiplicity dependence of light nuclei production at LHC energies in the canonical statistical model. *Phys. Lett. B* **785**, 171 (2018).
37. Andronic, A. *et al.* Decoding the phase structure of QCD via particle production at high energy. *Nature* **561**, 321 (2018).
38. Oliinychenko, D. *et al.* Microscopic study of deuteron production in PbPb collisions at $\sqrt{s_{NN}} = 2.76$ TeV via hydrodynamics and a hadronic afterburner. *Phys. Rev. C* **99**, 044907 (2019).
39. Bellini, F. & Kalweit, A. P. Testing production scenarios for (anti-)(hyper-)nuclei and exotica at energies available at the CERN Large Hadron Collider. *Phys. Rev. C* **99**, 054905 (2019).
40. Sa, B. H. *et al.* PACIAE 2.0: An updated parton and hadron cascade model (program) for the relativistic nuclear collisions. *Comput. Phys. Commun.* **183**(2), 333 (2012).
41. Yan, Y. L. *et al.* Predictions for the production of light nuclei in *pp* collisions at $\sqrt{s} = 7$ and 14 TeV. *Phys. Rev. C* **85**, 024907 (2012).
42. Wang, J. L. *et al.* The energy dependence of antiparticle to particle ratios in high energy pp collisions. *Int. J. Mod. Phys. E* **23**(12), 1450088 (2014).
43. Chen, G. *et al.* Antimatter production in central Au + Au collisions at $\sqrt{s_{NN}} = 200$ GeV. *Phys. Rev. C* **86**, 054910 (2012).
44. Chen, G. *et al.* Centrality dependence of light (anti)nuclei and (anti)hypertriton production in Au + Au collisions at $\sqrt{s_{NN}} = 200$ GeV. *Phys. Rev. C* **88**, 034908 (2013).
45. Chen, G. *et al.* Scaling properties of light (anti)nuclei and (anti)hypertriton production in Au + Au collisions at $\sqrt{s_{NN}} = 200$ GeV. *J. Phys. G: Nucl. Part. Phys.* **41**(11), 115102 (2014).

46. She, Z. L. *et al.* Centrality dependence of light (anti)nuclei and (anti)hypertriton production in Pb–Pb collisions at $\sqrt{s_{NN}} = 2.76$ TeV. *Eur. Phys. J. A* **52**(4), 93 (2016).
47. Dong, Z. J. *et al.* Energy dependence of light (anti)nuclei and (anti)hypertriton production in the Au–Au collision from $\sqrt{s_{NN}} = 11.5$ to 5020 GeV. *Eur. Phys. J. A* **54**(9), 144 (2018).
48. Liu, F. X. *et al.* ${}^{3}_{\Lambda}\mathrm{H}$ and ${}^{\overline{3}}_{\overline{\Lambda}}\overline{\mathrm{H}}$ production and characterization in Cu + Cu collisions at $\sqrt{s_{NN}} = 200$ GeV. *Phys. Rev. C* **99**, 034904 (2019).
49. Liu, F. X. *et al.* Light (anti)nuclei production in Cu + Cu collisions at $\sqrt{s_{NN}} = 200$ GeV. *Eur. Phys. J. A* **55**(9), 160 (2019).
50. Sa, B. H. *et al.* PACIAE 2.1: An updated issue of the parton and hadron cascade model PACIAE 2.0. *Comput. Phys. Commun.* **184**, 1476 (2013).
51. Zhou, D. M. *et al.* An upgraded issue of the parton and hadron cascade model, PACIAE 2.2. *Comput. Phys. Commun.* **193**, 89 (2015).
52. Sjöstrand, T., Mrenna, S. & Skands, P. PYTHIA 6.4 physics and manual. *J. High Energy Phys.* **2006**(05), 026 (2006).
53. Combridge, B., Kripfganz, J. & Ranft, J. Hadron production at large transverse momentum and QCD. *Phys. Lett. B* **70**(2), 234 (1977).
54. Yan, Y. L. *et al.* Announcement for the replacement of the PACIAE 2.1 and PACIAE 2.2 series. *Comput. Phys. Commun.* **224**, 417 (2018).
55. Ma, G. L. & Zhang, B. Effects of final state interactions on charge separation in relativistic heavy ion collisions. *Phys. Lett. B* **700**, 39 (2011).
56. She, Z. L. *et al.* Predictions for production of ${}^{3}_{\Lambda}\mathrm{H}$ and ${}^{\overline{3}}_{\overline{\Lambda}}\overline{\mathrm{H}}$ in isobaric ${}^{96}_{44}\mathrm{Ru}+{}^{96}_{44}\mathrm{Ru}$ and ${}^{96}_{40}\mathrm{Zr}+{}^{96}_{40}\mathrm{Zr}$ collisions at $\sqrt{s_{\mathrm{NN}}} = 200$ GeV. *Phys. Rev. C* **103**, 014906 (2021).
57. Sa, B. H. *et al.* Towards a qualitative hadron–parton correspondence in the nuclear modification factor. arXiv:2010.14817.
58. Zhang, S. *et al.* Searching for onset of deconfinement via hypernuclei and baryon-strangeness correlations. *Phys. Lett. B* **684**, 224 (2010).
59. Andronic, A. *et al.* Production of light nuclei, hypernuclei and their antiparticles in relativistic nuclear collisions. *Phys. Lett. B* **697**, 203 (2011).
60. Stowe, K. *An Introduction to Thermodynamics and Statistical Mechanics* (Cambridge University Press, 2007).
61. Xu, H. G. *et al.* Investigation of Ω_c^0 states decaying to $\Xi_c^+ K^-$ in pp collisions at $\sqrt{s} = 7$, 13 TeV. *Phys. Rev. C* **102**, 054319 (2020).
62. Cronin, J. W. *et al.* Production of hadrons at large transverse momentum at 200, 300, and 400 Gev. *Phys. Rev. D* **11**, 3105 (1975).
63. Lv, M. *et al.* Nuclear modification factor in intermediate-energy heavy-ion collisions. *Phys. Lett. B* **733**, 105 (2014).
64. Rezaeian, A. H. & Lu, Z. Cronin effect for protons and pions in high-energy pA collisions. *Nucl. Phys. A* **826**, 198 (2009).
65. Polleri, A., Bondorf, J. P. & Mishustin, I. N. Effects of collective expansion on light cluster spectra in relativistic heavy ion collisions. *Phys. Lett. B* **419**, 19 (1998).

Acknowledgements

The work of F. X. Liu is supported by the Program for Excellent Talents in Hubei Polytechnic University (21xjz22R, 21xjz21R), of D. M. Zhou is supported by the National Natural Science Foundation of China (11705167), and of G. Chen is supported by the National Natural Science Foundation of China (11475149).

Author contributions

Z.-L.S., G.C., D.-M.Z. put forward the problem and write the calculation program; F.-X.L. and H.-G.X. calculated data and plotted figures; F.-X.L. and Z.-L.S. write the draft; Z.-L.S., G.C., D.-M.Z., B.-H.S. revised the first draft and finished the final manuscript. All authors reviewed the manuscript.

Competing interests

The authors declare no competing interests.

Additional information

Correspondence and requests for materials should be addressed to Z.-L.S.

Reprints and permissions information is available at www.nature.com/reprints.

Publisher's note Springer Nature remains neutral with regard to jurisdictional claims in published maps and institutional affiliations.